JARQ 41 (1), 53 – 64 (2007) http://www.jircas.affrc.go.jp

Evaluation of CFD Accuracy for the Ventilation Study of a Naturally Ventilated Broiler House

In-Bok LEE[1], Sadanori SASE[2]* and Si-Heung SUNG[3]

[1] Department of Rural System Engineering, Seoul National University (Seoul 151–742, Korea)
[2] Department of Rural Technologies, National Institute for Rural Engineering (Tsukuba, Ibaraki 305–8609, Japan)
[3] Department of Biosystems Engineering, Konkuk University (Chungju 380–701, Korea)

Abstract

Using the CFD model, a new ventilation system design will be found later taking into consideration the ventilation efficiency such as uniformity, stability, and suitability of environmental factors in a naturally ventilated broiler house. Because conducting a field experiment for the ventilation study presented so many difficulties, a reliable 3-dimentional computational fluid dynamics (CFD) model had to be developed to investigate the natural ventilation. Before investigating its accuracy, a wind tunnel and particle image velocimetry (PIV) test was initially conducted to find their best experimental conditions and improve the PIV accuracy[13,15]. A 1/20 scale model of a naturally ventilated broiler house was used to get qualitative and quantitative airflow distribution in the broiler house using the PIV and CFD. To improve the CFD accuracy, the PIV and CFD computed airflows in the broiler house were compared, particularly on the distribution, local air velocity, and turbulent intensity in the house. The quality of the mesh density and the design of the boundary condition, especially the wind velocity and turbulence profiles, were found to be very important for getting accurate results. Assuming the PIV results were accurate, the most accurate CFD results were obtained when using a RNG k-ε turbulence numerical model. The average error of the CFD computed air velocity when using the RNG k-ε models was -6.2%.

Discipline: Agriculture facilities
Additional key words: aerodynamics, computational fluid dynamics, natural ventilation, particle image velocimetry, wind tunnel

Introduction

More than 87% of the broiler houses in Korea is naturally ventilated having double-winch curtained side vent openings without using any fan, and only circulating fans are used in the houses for hot seasons[16]. Their poor ventilation systems have seasonally caused the trouble of maintaining environmental control such as suitability, stability, and uniformity of the internal climate, causing serious stress on chickens, difficult disease control, and decreased productivity. Even though the broiler houses have been modernized, their internal climates have not been greatly improved yet because they have become larger and larger in consideration of automation and high productivity.

Choi et al.[2] measured air temperature, relative humidity, gas concentrations, weight of chickens, SDS (sudden death syndrome) and death rates, and so on in several typical types of broiler houses in Korea. Hwang et al.[7] and Yu et al.[22] conducted field experiments at commercial broiler houses in Korea to study the ventilation effects on the internal climate condition, however, those experiments were conducted in a single season and the measurement points were very limited in the house. It means that their data could not be effectively used to study the uniformity, stability, and suitability of the internal climate. Moreover, they did not present any upgraded design of the ventilation. Accordingly, there was a very urgent need to upgrade the ventilation systems of broiler houses for the four distinguished seasons of the Korean climate. However, ventilation studies have not been actively conducted yet because of many difficulties associated with conducting field experiments at the houses[14]. The main

This paper reports the results obtained in the Korea-Japan joint project on “Structural design and environmental control of large-sized agricultural buildings by latest aerodynamic techniques”.
*Corresponding author: fax +81–29–838–7609; e-mail sase@affrc.go.jp
Received 28 October 2005; accepted 9 May 2006.

reason was that most field experiments have been conducted with very limited measurement points as well as that the weather condition is always very unstable and unpredictable making it impossible to control artificially.

Computational fluid dynamics (CFD) has been one of the most powerful and handy tools for studying aerodynamics in agriculture[9,18]. It is often the most rapid, economical, and accurate means to support design decisions dealing with the full complexity of a real fluid flow. It can be used for early design cycles while providing a large amount of reliable data. However, the CFD accuracy is strongly dependent on the designer's skill, experience, and knowledge. Accordingly, the increasing number and increasing quality of numerical calculations of flow fields require more adequate and reliable data for examining the CFD validation in order to decide whether the physics of the problem has been modeled correctly[10].

The particle image velocimetry (PIV) can be a valuable tool in studying flow fields in agricultural structures and in investigating the accuracy of the numerical simulation. PIV can be assumed to be more accurate than the CFD because it tracks smoke particles or other media in the air directly and so it precisely captures the flow velocity of full flow fields[12,17]. The wind tunnel is a device used to artificially control airflow. It produces a controlled stream of air and is used to study the effects of air on moving objects such as aircraft or on stationary objects such as buildings. Compared with field experiments using full-scale objects, wind tunnel tests typically use small-scale models. These models make it possible for the designer to easily change the shape or size of the object and then analyze the data, while maintaining stable and identical wind characteristics. This method lowers the cost and produces a large volume and range of data in a short time. However, the dimension difference between the full- and small-scale models, airflow characteristics, data collection time, and so on, should be carefully managed to improve the accuracy of the wind tunnel results.

The overall objective of this study was to develop a CFD model (Fluent Inc., Lebanon, NH, USA) for studying the natural ventilation characteristics of a naturally ventilated broiler house, a typical model in Korea, and to improve the CFD performance and accuracy using the aerodynamic results of wind tunnel and PIV (TSI Inc., St. Paul, MN, USA). For this study, the wind and turbulence profiles (20–30% of turbulent intensity) were already designed in the test section of the wind tunnel using the log-term measured data[13]. Detailed modeling of each CFD parameter and mesh design was carefully performed to improve the CFD accuracy and then the optimum options for each parameter were finally established.

Materials and methods

1. Experimental facilities

(1) Wind tunnel system

The National Institute of Agricultural Engineering (NIAE) in Korea built a multi-purpose, large-sized wind tunnel (open-return type) on 24 November 2002 as shown in Fig. 1. The wind tunnel was an Eiffel type and the dimension of the test section was 2.0 × 1.7 × 15.0 m. The entire length of the wind tunnel, including the 15-m test section, was 28.5 m. Lee et al.[13] presented more detailed information of the wind tunnel.

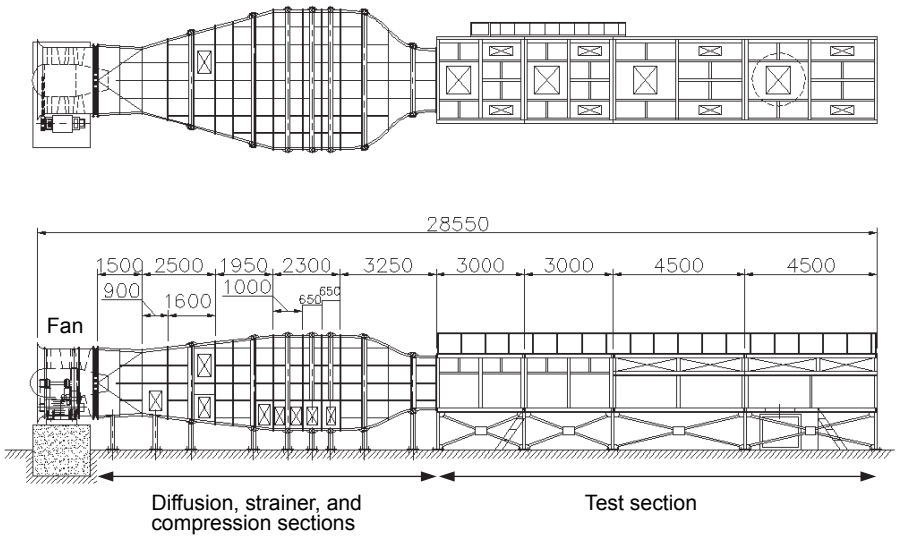

Fig. 1. Plane and side figures of the wind tunnel at the NIAE, Korea (unit: mm)

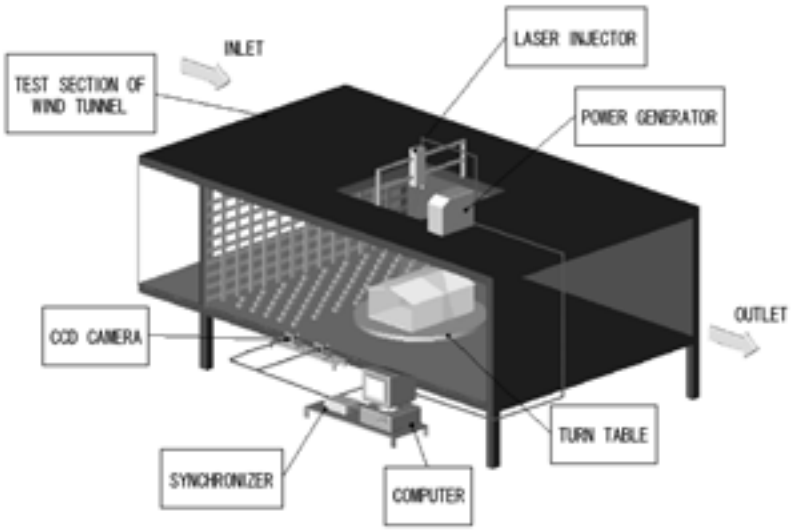

Fig. 2. Schematic diagram of the test section of the wind tunnel, including the PIV system and tools of lattice and blocks for profile design

(2) Particle image velocimetry

The ability to see flow patterns in and around a device under investigation often gives an insight into a solution to an aerodynamic problem[1]. While flow visualization is a very important part of wind tunnel testing, it is very difficult to use anemometer sensors because they are difficult to install and they may interrupt the natural airflow pattern. In this study, it was assumed that the PIV could overcome this problem. Figure 2 shows the schematic diagram of the PIV setup in the test section of the wind tunnel. The PIV system included laser and light-sheet optics, an image capture/shifting component, synchronizer, and computer hardware/software. Lasers are widely used in PIV because of their ability to emit monochromatic light with high-energy density, which can easily be bundled into thin light sheets for illuminating and recording the tracer particles without chromatic aberrations[21]. The detailed explanation of the PIV system was presented in Lee et al.[11,12] and Zhao et al.[23].

(3) Computational fluid dynamics

The Fluent commercial CFD program (Version 6.0, Fluent Inc., New Hampshire, USA) was used for this study. The CFD technique numerically solved the Reynolds-averaged form of the Navier-Stokes equations[8,10] within each cell in the domain. The equations were discretized on a curvilinear grid to be able to compute in complex and irregular geometries. The Reynolds-averaged process considered the instantaneous fluid velocity to be the sum of a mean and a fluctuating component of turbulence. The mass (1), continuity (2), and energy (3) conservation equations are shown as follows:

$$\frac{\partial \rho}{\partial t} + \frac{\partial}{\partial x_i}(\rho u_i) = S_m \quad (1)$$

$$\frac{\partial}{\partial t}(\rho u_i) + \frac{\partial}{\partial x_i}(\rho u_i u_i) = -\frac{\partial p}{\partial x_i} + \frac{\partial \tau_{ij}}{\partial x_j} + \rho g_i + F_i \quad (2)$$

$$\frac{\partial}{\partial t}(\rho h) + \frac{\partial}{\partial x_i}(\rho u_i h) = \frac{\partial}{\partial x_i}\left(K \frac{\partial T}{\partial x_i}\right) - \frac{\partial}{\partial x_i}\sum_j h_j J_j + \frac{\partial p}{\partial t} + u_i \frac{\partial p}{\partial x_i} + \tau_{ij} \frac{\partial u_i}{\partial x_j} + S_h \quad (3)$$

where F_i: external force vector (N m^{-3}), g_i: gravitational acceleration (m s^{-2}), J_j: component of diffusion flux (kg m^{-2} s^{-1}), h: specific enthalpy (J kg^{-1}), K: thermal conductivity (W m^{-1} K^{-1}), p: pressure (Pa), S_m: mass source (kg m^{-3} s^{-1}), S_h: total entropy (J K^{-1}), T: temperature (K), t: time (s), u_i: component of velocity (m s^{-1}), x_i: component of length (m), ρ: fluid density (kg m^{-3}), τ_{ij}: stress tensor (Pa).

The study used Fluent Version 6.0's typical turbulence numerical models[4] to find the most appropriate turbulence model for natural ventilation of a naturally ventilated broiler house. These typical models were the Standard k-ε, Renormalization-group (RNG) k-ε, Realizable k-ε, and Reynolds stress model (RSM). The Standard, RNG, and Realizable k-ε models have similar forms, with transport equations for k and ε. As shown in Table 1, the major differences in the models are the methods of calculating turbulent viscosity, the turbulent Prandtl numbers governing the turbulent diffusion of k and ε, and the generation and destruction terms in the ε equation.

Table 1. The comparison of transport equations for turbulence characteristics (Fluent, 2004)

Standard k-ε turbulence model	$\rho \frac{Dk}{Dt} = \frac{\partial}{\partial x_i}\left[\left(\mu + \frac{\mu_t}{\sigma_k}\right)\frac{\partial k}{\partial x_i}\right] + G_k + G_b - \rho\varepsilon - Y_M$ $\rho \frac{D\varepsilon}{Dt} = \frac{\partial}{\partial x_i}\left[\left(\mu + \frac{\mu_t}{\sigma_\varepsilon}\right)\frac{\partial \varepsilon}{\partial x_i}\right] + C_{1\varepsilon}\frac{\varepsilon}{k}(G_k + C_{3\varepsilon}G_b) - C_{2\varepsilon}\rho\frac{\varepsilon^2}{k}$ $C_{1\varepsilon}$ (1.44), $C_{2\varepsilon}$ (1.92), C_μ (0.09), σ_k (1.0), σ_ε (1.3)
RNG k-ε model	$\rho \frac{Dk}{Dt} = \frac{\partial}{\partial x_i}\left(\alpha_k \mu_{eff}\frac{\partial k}{\partial x_i}\right) + G_k + G_b - \rho\varepsilon - Y_M$ $\rho \frac{D\varepsilon}{Dt} = \frac{\partial}{\partial x_i}\left(\alpha_\varepsilon \mu_{eff}\frac{\partial \varepsilon}{\partial x_i}\right) + C_{1\varepsilon}\frac{\varepsilon}{k}(G_k + C_{3\varepsilon}G_b) - C_{2\varepsilon}\rho\frac{\varepsilon^2}{k} - R$ $C_{1\varepsilon}$ (1.42), $C_{2\varepsilon}$ (1.68)
Realizable k-ε model	$\rho \frac{Dk}{Dt} = \frac{\partial}{\partial x_j}\left[\left(\mu + \frac{\mu_t}{\sigma_k}\right)\frac{\partial k}{\partial x_j}\right] + G_k + G_b - \rho\varepsilon - Y_M$ $\rho \frac{D\varepsilon}{Dt} = \frac{\partial}{\partial x_j}\left[\left(\mu + \frac{\mu_t}{\sigma_\varepsilon}\right)\frac{\partial \varepsilon}{\partial x_j}\right] + \rho C_1 S\varepsilon - \rho C_2 \frac{\varepsilon^2}{k + \sqrt{\nu\varepsilon}} + C_{1\varepsilon}\frac{\varepsilon}{k}C_{3\varepsilon}G_b$ $C_{1\varepsilon}$ (1.44), $C_{2\varepsilon}$ (1.9), σ_k (1.0), σ_ε (1.2)
Reynolds stress model (RSM)	$\frac{\partial}{\partial t}\left(\rho\overline{u_i u_j}\right) + \frac{\partial}{\partial x_k}\left(\rho U_k \overline{u_i u_j}\right) = -\frac{\partial}{\partial x_k}\left[\rho\overline{u_i u_j u_k} + \overline{p\left(\delta_{kj}u_i + \delta_{ik}u_j\right)}\right]$ $+\frac{\partial}{\partial x_k}\left[\mu\frac{\partial}{\partial x_k}\left(\overline{u_i u_j}\right)\right] - \rho\left(\overline{u_i u_k}\frac{\partial U_j}{\partial x_k} + \overline{u_j u_k}\frac{\partial U_i}{\partial x_k}\right) - \rho\beta\left(g_i\overline{u_j\theta} + g_j\overline{u_i\theta}\right)$ $+\overline{p\left(\frac{\partial u_i}{\partial x_j} + \frac{\partial u_j}{\partial x_i}\right)} - 2\mu\overline{\frac{\partial u_i}{\partial x_k}\frac{\partial u_j}{\partial x_k}} - 2\rho\Omega_k\left(\overline{u_j u_m}\varepsilon_{ikm} + \overline{u_i u_m}\varepsilon_{jkm}\right)$

$C_{1\varepsilon}$, $C_{2\varepsilon}$: constant.

$C_{3\varepsilon}$: $\tanh\left|\frac{u_1}{u_2}\right|$.

u_1 and u_2 are the components of the flow velocities parallel and perpendicular, respectively to the gravitational vector.

G_b : generation of kinetic energy due to the buoyancy (kg m^{-1} s^{-2}).

G_k : generation of turbulent kinetic energy due to the mean velocity gradients (kg m^{-1} s^{-2}).

k : turbulent kinetic energy (m^2 s^{-2}).

p : pressure (Pa).

R : gas-law constant (8.31447 × 10^3 J kgmol^{-1} K^{-1}).

S : mean strain rate (m^2 s^{-2}).

t : time (s).

u_i, u_j, u_k, u_m : component of fluctuating velocity (m s^{-1}).

U_i, U_j, U_k : component of mean velocity (m s^{-1}).

x_i : component of length (m).

Y_M : contribution of the fluctuating dilatation in compressible turbulence to the overall dissipation rate (kg m^{-1} s^{-2}).

α_ε : generation of kinetic energy due to buoyancy (kg m^{-1} s^{-2}).

α_k : generation of kinetic energy due to the mean velocity gradients (kg m^{-1} s^{-2}).

β : coefficient of thermal expansion (K^{-1}).

δ : Kronecker delta function.

ε : turbulent dissipation rate (m^2 s^{-3}).

ρ : density (kg m^{-3}).

μ : viscosity (m^2 s).

μ_{eff} : effective viscosity ($\mu+\mu_t$).

μ_t : turbulent viscosity (m^2 s).

ν : molecular kinetic viscosity (μ/ρ).

σ_k : the turbulent Prandtl number for k.

σ_ε : the turbulent Prandtl number for ε.

Ω : mean-rate-rotation tensor (m^2 s^{-2}).

Ω_k : angular velocity for the reference frame.

Subscripts

i, j, k, m : direction vector index (= 1, 2, 3).

The Standard k-ε turbulence model is the simplest of the two-equation turbulence models in which the solution of two separate transport equations allows the turbulent velocity and length scales. The turbulent kinetic energy, k, and its rate of dissipation, ε are obtained from the transport equations shown in Table 1. The RNG k-ε model is similar in form to the Standard k-ε model. However, the RNG theory provides an analytical formula for turbu-

lent Prandtl numbers, while the Standard k-ε model uses user-specified, constant values. While the Standard k-ε model is a high Reynolds-number model, the RNG theory provides an analytically derived differential formula for effective viscosity that accounts for low Reynolds-number effects. Considering the Realizable k-ε model, the term "realizable" means that the model satisfies certain mathematical constraints on the Reynolds stresses, it is consistent with the physics of turbulent flows.

The RSM is one of the most elaborate turbulence models. Abandoning the isotropic eddy-viscosity hypothesis, the RSM closes the Reynolds-averaged Navier-Stokes equations by solving transport equations for the Reynolds stresses, together with equations for the dissipation rate. This means that four additional transport equations are required in 2-D flows and seven additional transport equations must be solved in three-dimensional flows. Compared with the k-ε models, the RSM requires additional memory and calculating time because of the increased number of the transport equations for Reynolds stresses.

2. Experimental procedures

Before the PIV and CFD airflow data were compared qualitatively and quantitatively, a wind tunnel and PIV test was performed to verify and improve the PIV accuracy. The accuracy of the PIV system installed at the wind tunnel of NIAE had been improved, and the results indicated an average PIV accuracy of 2.1% while the maximum error was 5.4%[15].

After improving the maximum PIV accuracy, the 2-D airflow patterns in a 1/20 scale, naturally ventilated broiler house (Fig. 3) were measured using the PIV when the wind speed was 1.5 m s^{-1} at 0.5 m above the floor perpendicular to the side wall of the broiler house model. Figure 4 shows the 1/20 scale model used for the wind tunnel test. It was made of acrylic panel having 3-mm thickness. Wings were installed at both the model's end walls to effectively prevent the air flowing between the end wall and the side wall of the wind tunnel's test section, which may affect the pressure distribution at the leeward side of the broiler house model. To obtain a flow field image with PIV, the laser was pulsed and the CCD video camera was triggered with the correct sequence and timing for the flow conditions (9 × 9 μm pixel size, 10 μs frame capture rate, 1,008 H × 1,018 W total pixels). The local displacement vector of the first and second illumination for the tracer particles' images was determined for each interrogation area by means of statistical methods (cross-correlation) using a 0.2 × 0.2 m window size and 0.25-second step. At this time, the distance between the CCD camera and the laser sheet location was 1.1 m.

For this study, the wind (Eq. (4)) and turbulence profiles (20–30% of turbulent intensity) had already been designed in the test section of the wind tunnel using the log-term measured data[13]. The wind profile was expressed

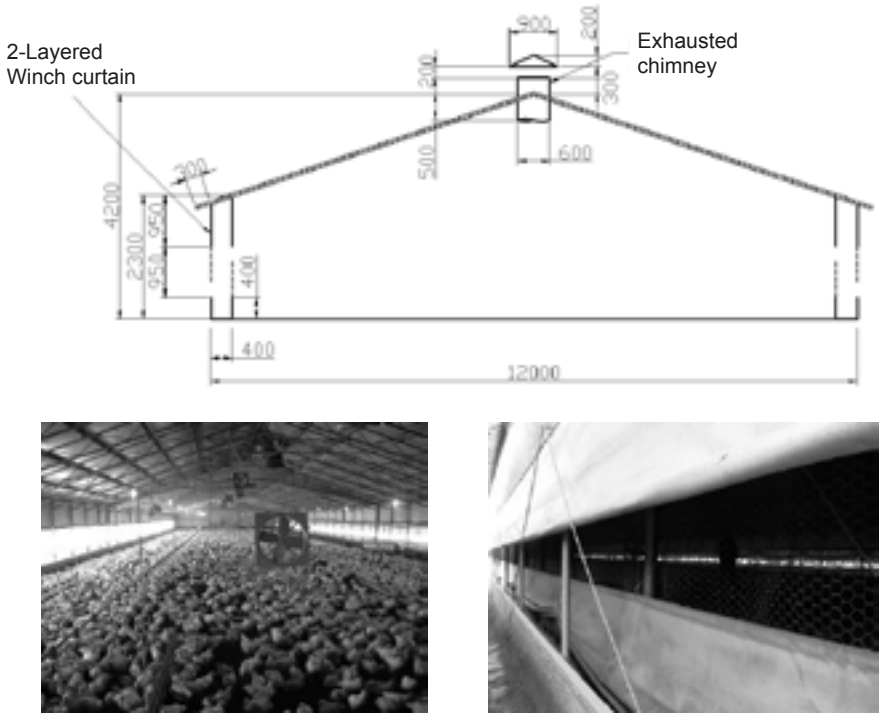

Fig. 3. Schematic diagram of a naturally ventilated broiler house used in this study

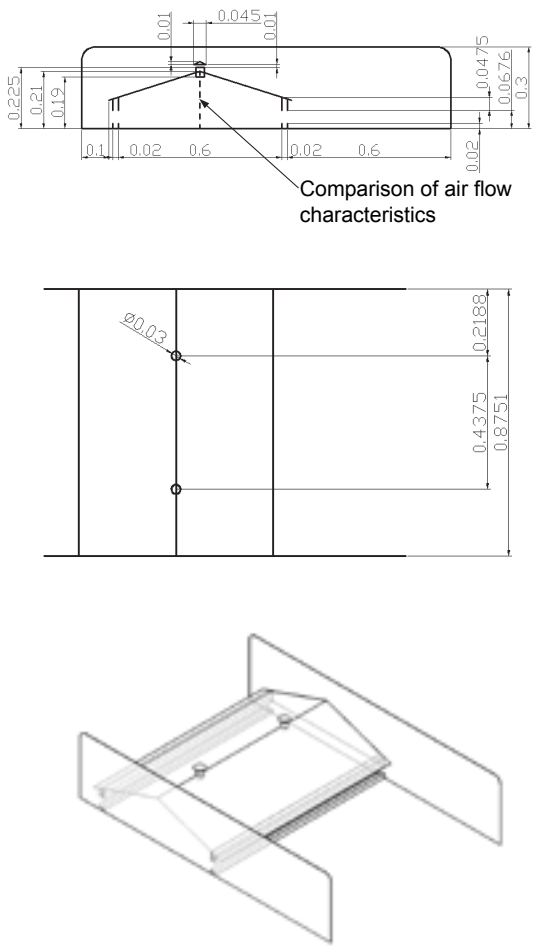

Fig. 4. A 1/20 scale model of the broiler house used for wind tunnel and PIV test

in terms of the velocity ratio of the variable height anemometer, compared with the fixed anemometer at 10 m in height. The detailed information of wind and turbulence profiles, considering a scale of 1/20, was presented in Lee et al.[13].

$$\frac{\bar{u}_z}{\bar{u}_{10}} = \frac{\log(z/z_0)}{\log(10/z_0)} \tag{4}$$

The term of z indicates height from the ground (m). Figure 5 shows the profiles of the wind velocity and the turbulent intensity used for this wind tunnel test. For the similarity of air velocity, the Froude number was used[3,20]:

$$\left(\frac{V^2}{gB}\right)_{model} = \left(\frac{V^2}{gB}\right)_{full} \tag{5}$$

where V, g, and B are air velocity (m s^{-1}), gravitational acceleration (m s^{-2}), and geometrical dimension of structure (m), respectively. While the CFD simulated the real broiler house and the PIV worked with its scale model, the Eq. (5) was used for the similarity of the PIV results.

To improve the CFD accuracy, the study exerted much effort to find the appropriate mesh quality and density, optimum setting condition of wind velocity and turbulence profiles, and optimum turbulent numerical model of the CFD program. The mesh quality is very important to get accurate data and computational convergence. Thus, the statistical distribution of mesh elements had to be investigated with respect to the specified quality criterion after the volume meshes were completed. As a normalized measure of the mesh elements' quality skewness, the Equiangle skew (Q_{EAS}) was used[4]:

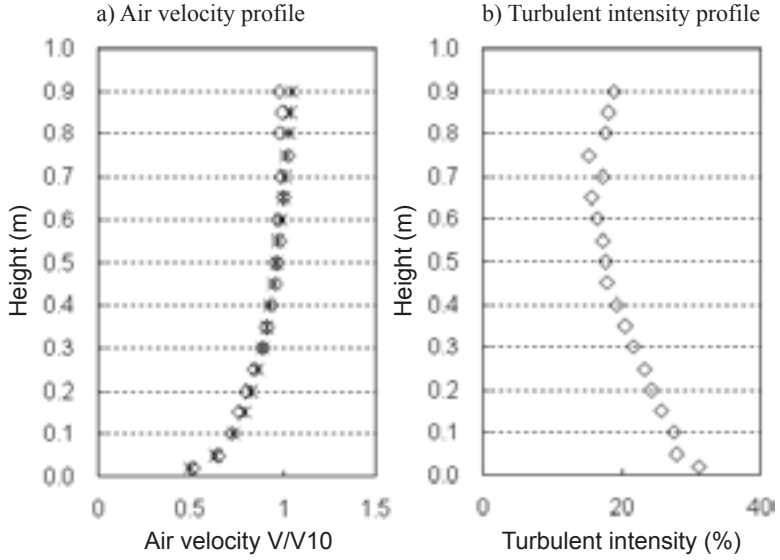

Fig. 5. Comparison of target (Eq. (4)) and measured profiles of wind velocity (a) and turbulence intensity (b) with the use of lattice and blocks when the wind speed at a height of 0.5 m in the test section was 1.5 m s^{-1} (Lee et al.[13])
◇: Measured, ∗: Target.

$$Q_{EAS} = \max\left\{\frac{\theta_{\max} - \theta_{eq}}{180 - \theta_{eq}}, \frac{\theta_{eq} - \theta_{\min}}{\theta_{eq}}\right\} \quad (6)$$

where θ_{max} and θ_{min} are the maximum and minimum angles (degrees) between the edges of the element, and θ_{eq} is the characteristic angle corresponding to an equilateral cell of similar form; for triangular and tetrahedral elements, θ_{eq} = 60; and for quadrilateral and hexahedral elements, θ_{eq} = 90. Q_{EAS} = 0 describes an equilateral element, and Q_{EAS} = 1 describes a completely degenerate (poorly shaped), equilateral element. In this study, a Q_{EAS} lower than 0.2 was assumed to be an excellent mesh quality[4]. After every volume of mesh generated, the study investigated the Equiangle skew of all volume mesh elements to find out if there was an area of poor mesh quality in the 3-D computational domain. Whenever a low-quality area was found, the study redesigned the mesh with different mesh shapes and mesh densities at the area.

It is an unfortunate fact that no single turbulence model is universally accepted as being superior for all classes of problems[4,5]. The typical turbulence numerical models provided by Fluent Version 6.0 were used for this study to find the most appropriate turbulence model for the natural ventilation of a multi-span greenhouse: Standard k-ε model, Renormalization-group (RNG) k-ε model, Realizable k-ε model, and Reynolds stress model (RSM). The Standard, RNG, and Realizable k-ε models have similar forms, with transport equations for k and ε. As shown in Table 1, the major differences in the models are the method of calculating turbulent viscosity, the turbulent Prandtl numbers governing the turbulent diffusion of k and ε, and the generation and destruction terms in the ε equation.

When the PIV and CFD computed results were compared with each other, the PIV and CFD computed airflow distribution (especially eddy location) at a cross-section plane of the broiler house was mainly compared with each other. As shown in Fig. 3, the vertical distribution of air velocities and turbulent intensities were also measured at the center of the broiler house using PIV and CFD and then compared with each other. The CFD boundary condition was specified as the same as the PIV and wind tunnel boundary condition (Table 2). The Froude number (Eq. (5)) was used for the similarity of air velocity of the wind tunnel test because a 1/20 scale model of the greenhouse was used for the PIV and wind tunnel test.

The vertical profiles of wind speed and turbulent intensity made in the wind tunnel were also programmed for the CFD model. The turbulence of the inlet airflow was specified using k and ε at each height of the profile as follows:

$$k = \frac{3}{2}(v \cdot I)^2 \quad (7)$$

$$\varepsilon = C_{\mu}^{3/4} \frac{k^{3/2}}{\gamma} \quad (8)$$

where k, v, I, ε, $C\mu$, and γ are turbulent kinetic energy (m^2 s^{-2}), air velocity (m s^{-1}), turbulent intensity (%), turbulent dissipation rate (m^2 s^{-3}), empirical constant (0.09), and turbulence length scale (m), respectively.

Results and discussion

1. Development of the CFD model

(1) Mesh design

The meshes were designed using Gambit, a Fluent CFD preprocessing program. Although designing it was very time consuming, it was one of the most important procedures to effectively increase the accuracy of CFD results. Unlike the CFD models developed for other engineering fields, the natural ventilation study of agricultural buildings requires a very big computational domain because a vertically and horizontally sufficient area should be secured around the broiler house, enough to make natural air flow. If the distance between the broiler house

Table 2. Main input values for the CFD model

Wind direction	Perpendicular to side wall
Wind speed	6.5 m s^{-1} at gutter height
Surface temperature of broiler house structure	23ºC
Surface temperature of floor	23ºC
Inlet air temperature	23ºC
Density of inlet air	1.1448 kg m^{-3}
Viscosity of inlet air	1.97×10^{-05} kg m^{-1} s^{-1}
Thermal conductivity of inlet air	0.0267 W m^{-1} ºC^{-1}
Specific heat of inlet air	1,007.2 J kg^{-1} ºC^{-1}
Gravitational acceleration	9.81 m s^{-2}
Atmospheric pressure	101,324 Pa

and the boundary walls of the computational domain was not sufficiently secured, the faster airflow stream could be compared with the natural airflow resulting in unreal airflow around the leeward vent opening. If the distance between the broiler house and the outlet of the computational domain was not enough, it would be very difficult to converge because of the effect of the backflow eddy developed at the leeward side of the structure. As one solution, the upper and side walls of the computational domain could be specified as the zero pressure region, however, it would not be the best solution because the convergence in this case would become very difficult.

In this study, it was impossible to design the whole broiler house having 70 m length in the computational domain considering the mesh number with computer capacity. As one solution, it was assumed that the internal airflow of the cross section was assumed to be uniform along the length of the broiler house while the external wind came to the side wall of the broiler house perpendicularly. Accordingly, the CFD model could be developed with only 17.5 m length of the broiler house. Moreover, comparing the airflow and pressure results of many CFD trials, it was found that the vertical and horizontal distance between the broiler house and the boundary wall of the computational domain should be kept at least 30 m.

The mesh type is very important for accurate CFD calculation. The meshes can be mainly composed of hexahedral and tetrahedral volume mesh elements for a 3-D computational domain. The tetrahedral volume element is very helpful to keep high-quality meshing for a complicatedly shaped region and to fit different-shaped regions, even though it requires many more meshes than the hexahedral mesh elements, resulting in increased file size and computational time. Because of the complicated shapes of the broiler house, the tetrahedral mesh volume element was used in this study. Accordingly, for this study's CFD model with a naturally ventilated broiler house, the mesh number was kept at a maximum of 298,600.

The computational domain was 92 × 30 × 17.5 m and the internal floor area measured 12 × 17.5 m. A uniformly designed mesh in the broiler house had a ratio of dimension of 0.35 while it was kept 0.2 at all vent openings. To get more accurate CFD results, the study found that meshes, especially those of various sizes, should be carefully designed. The airflow data in the broiler house is much more important than that of the external area, while the adjacent area of the broiler house is also very critical to make a reliable air pressure distribution around the structure. To effectively save the total mesh numbers, the dense meshes should be located in the broiler house model and the mesh size had to be designed gradually bigger as being far from the broiler house. The study also found that it was very critical not to make a big and sudden change of mesh size between adjacent meshes. It was assumed that the mesh quality including density and shape around the external surface of the broiler house model affected the external airflow and air pressure distribution of the broiler house, which greatly influenced the natural ventilation. Moreover, Fluent[4] insisted that rapid changes in cell volume between adjacent cells could translate into larger truncation errors. After the mesh densities in those areas were improved, the CFD model was assumed to more accurately predict the complex secondary airflow of natural ventilation involving the separation and recirculation of airflow[4]. Figure 6 shows the final computational grid for the CFD simulation. The mesh number of the broiler house volume was 85,567 while the total mesh number was 298,600 and the mesh type was tetrahedron.

The mesh quality is very important to get accurate data and the computational convergence. Thus, the statistical distribution of mesh elements had to be investigated with respect to the specified quality criterion after the volume meshes were completed. In this study, a Q_{EAS} lower than 0.2 was assumed to be an excellent mesh quality, as indicated in the Fluent manual[4]. After every volume mesh generation, the Equiangle skew of all volume mesh elements was investigated to find if there was an area of poor mesh quality in the 3-D computational domain. Whenever a low-quality area was found, the mesh was redesigned with different types of mesh shapes and mesh densities.

(2) Design of wind and turbulence profiles

The design of the vertical wind and turbulence profiles of the CFD model was also very important to improve the reality of the inlet boundary condition. Lee et al.[13] designed the wind and turbulence profiles for the wind tunnel and PIV test using the log-term measured field data of a typical rural area[6,19]. The same inlet boundary condition had to be specified at the CFD model to make an identical boundary condition for the CFD and PIV computation. The critical problem of the profile specification was how to keep the profile shapes unchanged while the air flows from the inlet of the computational domain to the broiler house location.

As shown in Fig. 7, if any procedure was not performed, the shapes of the wind and turbulence profiles were changed while the air flowed from the inlet of the computational domain to the broiler house location. To keep the profile shapes, an individual volume was developed between the inlet and just before the broiler house, and it was specified as the laminar flow zone to effectively maintain the profile shapes when the roughness of its floor was specified to be 0. Figure 7b shows the almost identical profiles after the treatment.

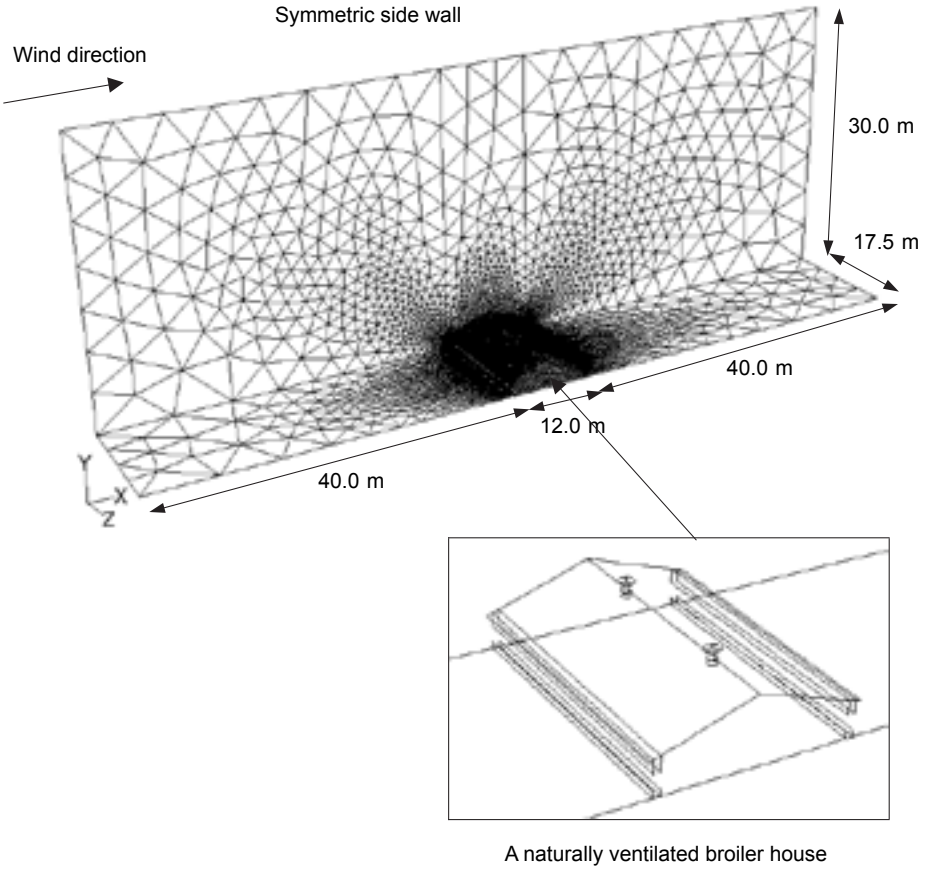

Fig. 6. Computational grid for the CFD simulation

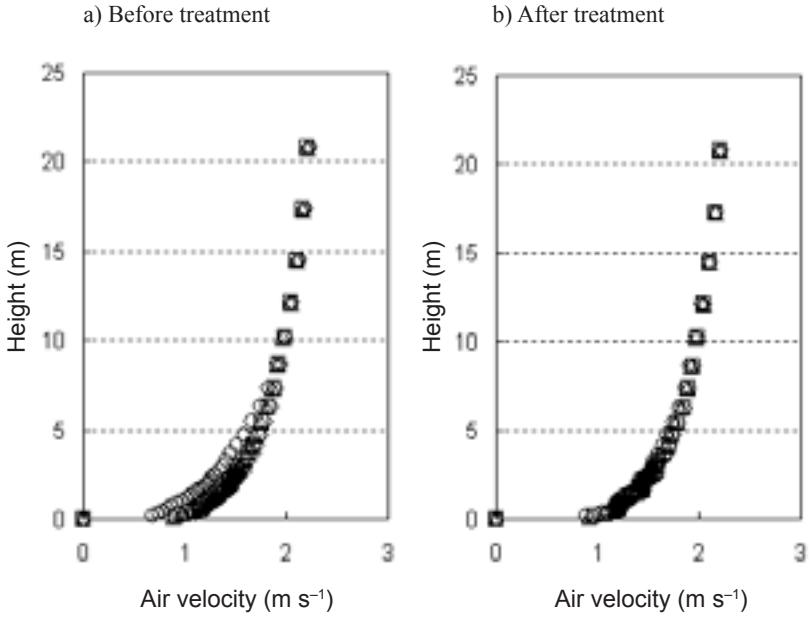

Fig. 7. The wind velocity profiles measured at 0.1, 5.0, 10.0, and 15.0 m from the inlet of the computational domain

◇: 0.1 m, □: 5.0 m, △: 10.0 m, ○: 15.0 m.

(3) Comparison of PIV and CFD results using turbulence models

Assuming that the mesh quality and profile design had been improved enough for the CFD calculation, the CFD models were computed with four distinguishable turbulence numerical models. To find the most appropriate turbulence model for the natural ventilation of a broiler house, this study used the typical turbulence numerical models, provided by Fluent Version 6.0, as stated earlier. The results of each CFD calculation were compared with the PIV computed airflow data measured at the wind tunnel. The distributions of local air velocity and turbulent intensity as well as the internal airflow distribution (particularly eddy center and separating location of airflow) were mainly compared quantitatively and qualitatively.

Figure 8 shows the vertical air velocity distribution of the PIV and CFD at the center of the broiler house shown in Fig. 4. The CFD-computed air velocities, using the turbulence numerical models, were compared with the PIV computed air velocity distribution vertically. Considering the PIV results, it was impossible to accurately compute the airflow near the floor because of severe laser reflections. The results showed a high airflow at the lower part of the broiler house, indicating that the windward side vent acted as the primary inlet. All the results indicated that the CFD got negative errors compared to the PIV even though positive errors were generated at the upper location, above 3.0 m height. The differences between the CFD computed air velocities above 3.0 m height were strongly dependent on the location of internal eddy that occurred below the roof. Comparing the PIV and CFD below 3.0 m height, the most accurate results were obtained when the RNG k-ε turbulence numerical model was used. When the RNG k-ε model was used, the average error was -6.2% while -14.4%, -25.6%, and -20.9% when using the Reynolds stress model, Standard k-ε model, and Realizable k-ε model, respectively.

Comparing the vertical air velocity distribution at the center of the broiler house shown in Fig. 9, the vertical distributions of the CFD computed turbulent intensity were shown to be very similar in shape to the PIV computed. Generally, the negative error was shown at the lower part while the positive error was shown at the center of the internal volume. The average errors of turbulent intensity when the RNG k-ε, Reynolds stress, Standard k-ε, and Realizable k-ε turbulence numerical models were used were 21.0%, 19.6%, 20.8%, and 10.9%, respectively. However, it was necessary to compare the negative and positive errors separately because those errors could be cancelled by each other for the overall error. The results of the Realizable k-ε model showed the lowest error even though the distribution was the most non-similar among the results of the turbulent models. When comparing the turbulent intensity at the main stream, the errors were shown to be -26.0%, -26.0%, -30.9%, and -42.0%, respectively. The Reynolds stress model had a much longer computational (iteration) time than the RNG k-ε model, because the RNG k-ε had fewer transport equations (total

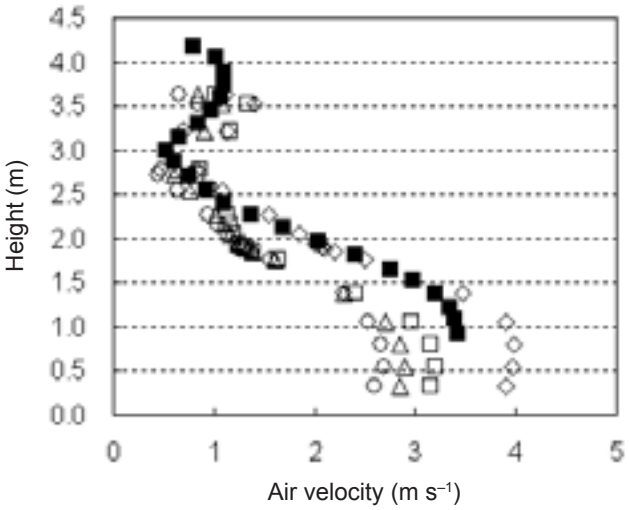

Fig. 8. Vertical distributions of CFD and PIV computed air velocity at the center of a naturally ventilated broiler house for an external wind speed of 6.5 m s^{-1} at a gutter height (wind direction from left to right)
◇: RNG, ○: Standard, △: Realized, □: Reynolds, ■: PIV.

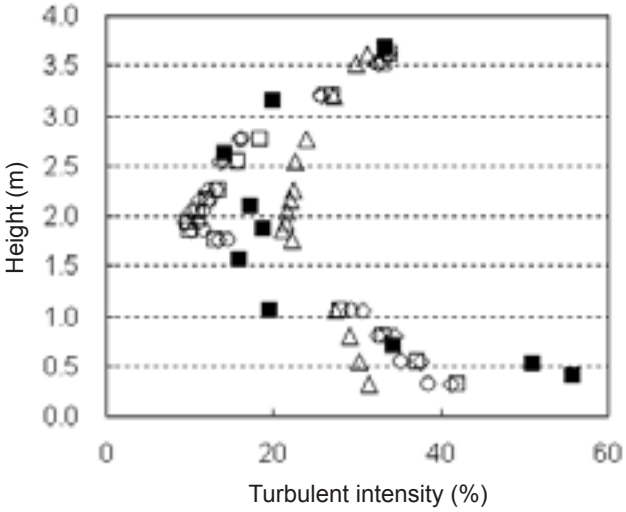

Fig. 9. Vertical distributions of CFD and PIV computed turbulent intensity at the center of a naturally ventilated broiler house for an external wind speed of 6.5 m s^{-1} at a gutter height (wind direction from left to right)
◇: RNG, ○: Standard, △: Realized, □: Reynolds, ■: PIV.

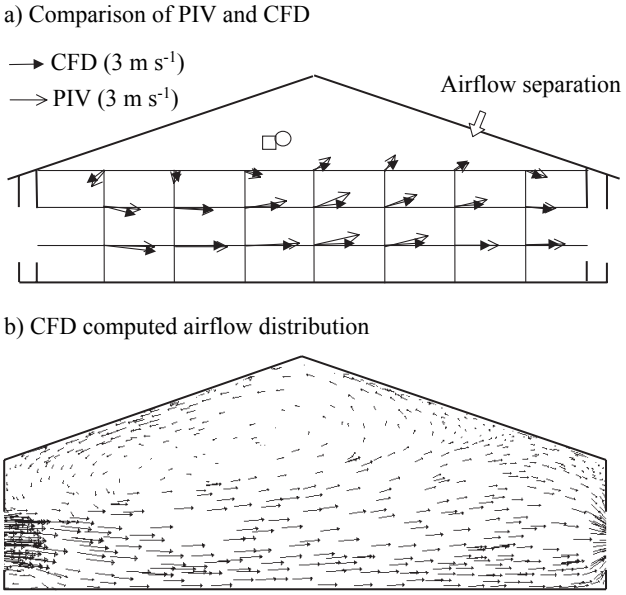

Fig. 10. Comparison of the PIV and CFD computed airflow distribution in a naturally ventilated broiler house for an external wind speed of 6.5 m s^{-1} at a gutter height (wind direction from left to right)

of two equations) than the Reynolds stress models (total of seven equations). Thus, considering the computational time, this study recommends the use of the RNG k-ε model for future ventilation studies of broiler houses.

The comparison of the PIV- and CFD-computed airflow distribution, when using the RNG k-ε model, is shown in Fig. 10. Considering the PIV results, it was impossible to compute the airflow near the floor because of severe laser reflections. The figures showed that the air entered the broiler house through the vent opening at the windward side, and then exited through the leeward side vent. It resulted in a counterclockwise internal airflow pattern at the center of the broiler house and the internal airflow patterns of the PIV and CFD were very similar. The locations of the eddy center below the roof and the airflow separation below the leeward roof were also shown to be very similar. The slight differences between the CFD and PIV computed local airflow directions were caused by the different locations of the eddy center below the roof. The symbols of (□) and (○) indicate the eddy center made by the PIV and CFD, respectively. Under the leeward roof, the airflow separation could be found at the same location of the PIV and CFD results. Like that of the PIV results, a much smaller eddy was also found just below the windward roof vent. Accordingly, the CFD computed airflow distribution could be very similar to that of the PIV.

Conclusions

Considering the mesh design, optimum turbulence model, profile maintenance, and inlet boundary condition, a CFD model was developed to study the natural ventilation of a broiler house using the aerodynamic results of wind tunnel and PIV. While a CFD model of a naturally ventilated broiler house was developed in this study, the information on the CFD design, like in all established designing procedures, can be used later to develop CFD tools that investigate the ventilation efficiency of naturally ventilated, typical Korean broiler houses.

The PIV and CFD results indicated that these techniques were effective methods for evaluating the relative performance of alternative designs of livestock house structures and air distribution patterns inside the buildings.

The CFD results showed that the appropriate mesh quality and density, profile design, and turbulence numerical model of the CFD program were very critical in improving the CFD accuracy. To effectively save the total mesh numbers, the dense meshes should be located in the broiler house model and the mesh size had to be designed gradually bigger as being far from the broiler house. The study also found that it was very critical not to make a big and sudden change of mesh size between adjacent meshes. To keep the profile shapes, an individual volume was developed between the inlet and just before

the broiler house, and it was specified as the laminar flow zone to effectively maintain the profile shapes when the roughness of its floor was specified to be 0.

Comparing the PIV and CFD air velocity distribution, the most accurate results were obtained when using the RNG k-ε turbulence numerical model, with the average error of -6.2%. However, it was not easy to effectively decrease the error of the turbulent intensity. It was finally found to be 26.0% when using the RNG k-ε turbulence numerical model. The internal airflow patterns of the PIV and CFD were very similar when the RNG k-ε turbulence numerical model was used. The locations of the eddy center below the roof vent and the airflow separation below the leeward roof were also clearly shown to be very similar.

References

1. Barlow, J. B., Rae, W. H. & Pope, A. (1999) *Low-speed wind tunnel testing* (3rd ed.). John Wiley & Sons, New York, USA, pp.545.
2. Choi, H. C. et al. (1999) Effect of housing and production systems on environment and performances in broiler production. *Kor. Soc. Livest. Housing Environ.*, **5**(2), 87–92.
3. Cook, N. J. (1997) *The designer's guide to wind loading of building structures part 2*. Butterworths Co., Croydon, UK, pp.1045.
4. Fluent Inc. (2004) The manual of computational fluid dynamics (CFD), version 5.5. New Hampshire, USA.
5. Hinze, J. O. (1975) *Turbulence* (2nd ed.). McGraw-Hill Inc., New York, USA, pp.398.
6. Hoxey, R. P. & Richards, P. J. (1992) Structure of the atmospheric boundary layer below 25 m and implications to wind loading on low-rise buildings. *J. Wind Eng. & Ind. Aerodynamics*, **41–44**, 317–327.
7. Hwang, B. et al. (2002) Study on environmental efficiency of windowless broiler house. *Kor. Soc. Anim. Sci. & Technol*., **44**(4), 475–482.
8. Launder, B. E. & Spalding, D. B. (1974) The numerical computation of turbulent flows. *Comput. Methods in Appl. Mech. & Eng.*, **3**(2), 269–289.
9. Lee, I. et al. (2000) Evaluation of structural characteristics of naturally ventilated multi-span greenhouses using computer simulation. *JARQ*, **34**(4), 247–256.
10. Lee, I. & Short, T. H. (2001) Verification of computational fluid dynamic temperature simulations in a full-scale naturally ventilated greenhouse. *Trans. ASAE*, **44**(1), 119–127.
11. Lee, I. et al. (2001) Performance of particle image velocimetry (PIV) for aerodynamic study of natural ventilation in large-sized multi-span greenhouses. ASAE Paper No. 014055, ASAE, St. Joseph, USA.
12. Lee, I. et al. (2003) A wind tunnel study of natural ventilation for multi-span greenhouse scale models using two-dimensional particle image velocimetry (PIV). *Trans. ASAE*, **46**(3), 763–772.
13. Lee, I. et al. (2004a) Development of vertical wind and turbulence profiles of wind tunnel boundary layers. *Trans. ASAE*, **47**(5), 1717–1726.
14. Lee, I. et al. (2004b) Study on forced ventilation system of a piglet house. *JARQ*, **38**(2), 81–90.
15. Lee, I. et al. (2005) PIV verification of greenhouse ventilation air flows to evaluate CFD accuracy. *Trans. ASAE*, **48**(6), 2277–2288.
16. NAQS (2003) Survey on livestock products. National Agricultural Products Quality Management Service (NAQS), Suwon, Korea, 117–140.
17. Raffel, M., Willert, C. E. & Kompenhans, J. (1998) *Particle image velocimetry*. Springer, New York, USA, pp.515.
18. Reichrath, S. & Davies, T. W. (2002) Using CFD to model the internal climate of greenhouses: past, present and future. *Agron.*, **22**, 3–19.
19. Richardson, G. M. & Blackmore, P. A. (1995) The Silsoe structures building: comparison of 1:100 model-scale data with full-scale data. *J. Wind Eng. & Ind. Aerodynamics*, **57**, 191–201.
20. Simiu, E. & Scanlan, R. H. (1996) *Wind effects on structures*. John Wiley & Sons, New York, USA, pp.466.
21. TSI Inc. (2003) The manual of particle image velocimetry (PIV) (2nd ed.). TSI Inc., St. Paul, USA.
22. Yu, B. et al. (2002) Study on the status of ventilation system for air intake from pipes beneath the gable with central chimney exhaust type of broiler chicken house. *In* Proceedings of Winter Meeting of the Kor. Soc. for Livestock Housing and Environ., 69–75.
23. Zhao, L. et al. (1999) Development of particle image velocimetry techniques to measure room airflow patterns in ventilated airspaces. *Trans. Am. Soc. Heat. Refrig. Air Cond. Eng.*, **105**(2), 1098–1107, SE-99-17-02.